Geomorphology 118 (2010) 33–47

Contents lists available at ScienceDirect

Geomorphology

journal homepage: www.elsevier.com/locate/geomorph

# Quantifying sand storage capacity of large woody debris on beaches using LiDAR

Jordan B.R. Eamer, Ian J. Walker *

*Boundary Layer Airflow and Sediment Transport (BLAST) Laboratory, Department of Geography, University of Victoria, PO BOX 3060 STN CSC, Victoria, British Columbia, Canada V8W 3R4*

ARTICLE INFO

*Article history:*
Received 11 August 2009
Received in revised form 2 December 2009
Accepted 7 December 2009
Available online 16 December 2009

*Keywords:*
Large woody debris (LWD)
Foredune
LiDAR
Queen Charlotte Islands (Haida Gwaii)
Aeolian
Beach

ABSTRACT

The sedimentological role of large woody debris (LWD) on beaches is understudied and is relevant for the morphodynamics of sandy, high-energy beach–dune systems of the northeast Pacific Ocean. On the west coast of Canada, this debris consists largely of historical escape logs from the coastal logging industry. In areas with competent wind regimes, LWD can trap appreciable amounts of windblown sand in the backshore, which can alter beach–foredune sediment budgets and initiate incipient dune formation. As this additional store of sediment must be reworked first during high water events, it provides an important buffer that reduces erosion of established foredunes.

This study examines the morphology and sand storage capacity of three backshore LWD deposits of varying morphologies on northeastern Graham Island, Haida Gwaii (Queen Charlotte Islands) British Columbia, Canada. A new method was developed using coincident high spatial resolution LiDAR data and digital orthophotographs to derive DEMs for distinct ground cover classes (sand, LWD). These DEMs were then used to quantify relative storage capacities of LWD and sand in the backshore. Significant amounts of sand are stored within and around LWD on beaches in the study region. Existing storage quantities (above HHWMT) range from $9.19\times10^4$ to $1.39\times10^5$ kg m$^{-1}$ beach width or ~1.14 to 1.60 m storage depth. The same LWD deposits have a further potential storage capacity ranging from 1.04 to $1.70\times10^4$ kg m$^{-1}$ beach width or ~0.21 to 0.28 m depth. The relative storage capacity of these features is reflected in the backshore morphology of each site, with sediment transport further into the backshore dependent upon the morphology and relative in-filling of the log debris jam. With this additional sediment storage, log debris could enhance development of large incipient dunes in the backshore thereby buffering against increasing storminess and gradual sea-level rise in the region. As the use of precise LiDAR data is increasing in geomorphic research, the development of a verifiable methodology for estimating beach–dune storage volumes is timely.



## 1. Introduction

The sedimentological role of large woody debris (LWD) on beaches is an understudied aspect of coastal geomorphology. These features exert notable control on the morphodynamics of sandy, high-energy beach–dune systems of the northeast Pacific Ocean and provide distinct ecological habitat in coastal regions (Maser and Sedell, 1994). On the west coast of Canada, LWD deposits consist largely of historical escape logs from the coastal logging industry with smaller and locally significant contributions from landslides, coastal erosion or river transport (Walker and Barrie, 2006).

On beaches with appreciable aeolian sand transport, LWD deposits serve three key geomorphic functions (Walker and Barrie, 2006). First, LWD acts as an accretion anchor that, by increasing aerodynamic surface roughness to sediment-laden airflow, promotes accumulation of significant amounts of windblown sand in the backshore (Fig. 1). This store of sand and debris buffers the coast against erosion and must be reworked first during wave attack. Second, LWD deposits provide nuclei for incipient dune growth. If aeolian accretion continues without erosion by waves or high water levels, LWD deposits fill and vegetation eventually colonizes (Fig. 2). This may take months to years depending on LWD extent, sand supply, high water event frequency, and vegetation type. Unlike typical incipient foredunes (cf. Hesp, 1989), however, sizable dunes can develop within LWD without vegetation colonization. Third, sand-laden LWD deposits dam backshore river discharge serving to either create or preserve backshore swales and lakes. These lakes are common on driftwood-laden beaches (Fig. 3) and aeolian accretion is often the key to their development. In some cases where onshore sand supply is high, backshore lakes may eventually fill with sand. Rapid drainage and rupture of these lakes by erosion of the foredune via channel incision or wave erosion is also common.

Unlike research on the impacts of large woody debris in fluvial systems (e.g., Keller and Swanson, 1979; Nakamura and Swanson, 1993; Kail, 2003; Wallerstein and Thorne, 2004), the geomorphic significance of LWD in beach–dune systems has not been documented in peer-reviewed literature to date. Recently, remotely sensed, light detection and ranging (LiDAR) data have been used to assess volumetric and morphological changes in beach–dune systems (e.g., Brock et al., 2002;

* Corresponding author. Tel.: +1 250 721 7347; fax +1 250 721 6216.
*E-mail address:* ijwalker@uvic.ca (I.J. Walker).

0169-555X/$ – see front matter © 2009 Elsevier B.V. All rights reserved.
doi:10.1016/j.geomorph.2009.12.006

**Fig. 1.** Seaward margin of extensive backshore LWD deposit in the study region on Graham Island, Haida Gwaii, British Columbia, Canada. Strong onshore winds and high available sand supply have resulted in deposition of aeolian sand within the log matrix to form an unvegetated incipient foredune. Person holding survey rod for scale. Photo credit: I.J. Walker.

Saye et al., 2002; Woolard and Colby, 2002; Sallenger et al., 2003; Zhang et al., 2005). As LiDAR surveys can provide high-resolution topographic and often photogrammetric data for long, narrow, strips of terrain, their use for resolving coastal morphodynamic changes over a range of spatial scales is very effective. Brock et al. (2002), Sallenger et al. (2003) and Shrestha et al. (2005) all provide a useful account of data acquisition and processing for LiDAR surveys that were used for regional scale mapping of geomorphic change along sandy coasts in the United States in response to storms or longer-term coastal erosion and/or progradation. LiDAR surveys are also an extremely powerful tool when combined with other remote sensing techniques, such as multi- or hyperspectral imagery, to classify coastal land covers (e.g., Lee and Shan, 2003) or examine beach morphodynamics (e.g., Debruyn et al., 2006). Given the increasing use of LiDAR data in coastal geomorphology, there is a clear need for developing verifiable methodologies for the use of these data.

The purpose of this article is to examine the sediment storage capacity and morphodynamic implications of large woody debris deposits on beaches with high aeolian sand transport using LiDAR data from the coast of northern British Columbia, Canada. This purpose will be met via the following objectives. First, a simple and effective method is developed to use LiDAR data to quantify the storage capacity

**Fig. 2.** An incipient foredune developing within log debris seaward of an established foredune colonized with native dune grass (*Leymus mollis*). Photo credit: I.J. Walker.

**Fig. 3.** Sand-filled LWD deposit diverting stream discharge to form a backshore lake to the north of study site three. Outflow channel on beach is ~3 m wide for scale. Photo credit: K.I. Pearce.

of aeolian sand within LWD. This involves a supervised classification of high spatial resolution digital aerial photography to identify log and sand coverage within the imagery and assignment of co-located LiDAR elevation data to produce sand and drift log elevation surfaces. Second, data from the sand storage calculations, combined with aerial photography and ground surveys from three morphologically distinct study sites, are used to interpret the geomorphic significance of LWD within beach–dune systems and the broader scale implications for coastal sediment budgets.

## 2. Regional setting

### 2.1. Study area and environmental setting

The study area is located within Naikoon Provincial Park on northeastern Graham Island, Haida Gwaii (Queen Charlotte Islands), British Columbia, which is located approximately 80 km offshore from Prince Rupert (Fig. 4). Beaches in the study region are intermediate with multiple inter- to sub-tidal bars and a mixed sand to cobble sediment composition. The backshore is typically clad with LWD of varying size and density that consists mostly of felled timber logs >0.3 m in diameter with some localized deadfall from bluff erosion. Beaches are backed by low (5 to 10 m) bluffs and/or established foredunes (5 to 12 m high), blowouts, bluff-top dunes, and parabolic dunes.

The oceanographic setting in Hecate Strait is highly energetic, as characterized by a macro tidal range with highest high water mean tide (HHWMT) exceeding 7 m and an energetic wave climate with annual significant wave height, $H_s$, of 1.8 m with higher values exceeding 3.5 m along the shallower waters closer to the study area (East Beach) that prevail for 20–30% of the time during winter months (Walker and Barrie, 2006). Storm surges are also frequent in the region and the magnitude and occurrence of extreme annual water levels is strongly correlated to known climatic variability events, such as ENSO and the Pacific Decadal Oscillation (PDO) (Abeysirigunawardena and Walker, 2008).

The wind regime in the study area is highly competent and seasonally opposed with winds exceeding the conventional sand transport threshold of 6 m $s^{-1}$ (Bagnold, 1941) approximately 67% of the time at the Rose Spit meteorological station (Pearce, 2005; Walker and Barrie, 2006). The total aeolian sand drift potential of 3176 $m^3$ $m^{-1}$ $a^{-1}$ (Pearce, 2005) is well above those documented for the Canadian prairies (~ 300–1600 as per Wolfe and Lemmen, 1999) and is comparable to that of the Netherlands coast (~ 1700–4000 as per Tsoar, 2000). Despite high annual precipitation (~1400 mm $a^{-1}$), these winds move considerable amounts of littoral sediment onshore to maintain active foredune, blowout, and transgressive parabolic and bluff-top dunes. Recent aeolian process experiments (Pearce, 2005; Anderson and Walker, 2006) have shown that significant amounts of sediment (up to 110 kg $m^{-2}$) are transported as much as 300 m landward of the foredune during the fall–winter storm season resulting in several metres of vertical accretion and dune migration. These conditions produce a geomorphically dynamic beach–dune setting that, despite high aeolian activity, is retreating a rate of ~ 1 to 3 m $a^{-1}$ (Barrie and Conway, 2002).

The study area lies within the wet hyper-maritime subzone of the Coastal Western Hemlock Biogeoclimatic Zone and, as such, much of the inland consists of raised bogs interspersed with wetland forest. These areas host distinctive forest communities dominated by Sitka spruce (*Picea sitchensis*) and various herbaceous species including native dune grass (*Leymus mollis*), big-head sedge (*Carex macrocephala*), and invasive beach grasses (*Ammophila* spp.). Rapid colonization and stabilization of backshore dune systems is common in this eco-climatic setting and some vegetation colonization has occurred in the extensive LWD deposits on East Beach (Walker and Barrie, 2006).

### 2.2. Study site locations and rationale

Three study sites of different backshore and LWD morphologies were selected along East Beach (Figs. 4–7) to characterize a typical range of sand storage capacity in LWD in the study area (Table 1). Sites were chosen based on: i) the presence of extensive LWD that was recognizable in both LiDAR and digital aerial photograph coverage obtained in 2006, ii) ground surveys in 2005 through 2009, iii) the extent and density of LWD (e.g., areal extent, log density, amount of sediment deposition or burial), and iv) general site geomorphology (e.g., beach and LWD depths, alongshore continuity of sediment deposition, aeolian depositional and/or erosional features). Sites were generally an order of magnitude greater in shoreline length than cross-shore width (e.g., 800 to 1080 m long by 85 to 110 m wide). General site characteristics are provided in Table 1.

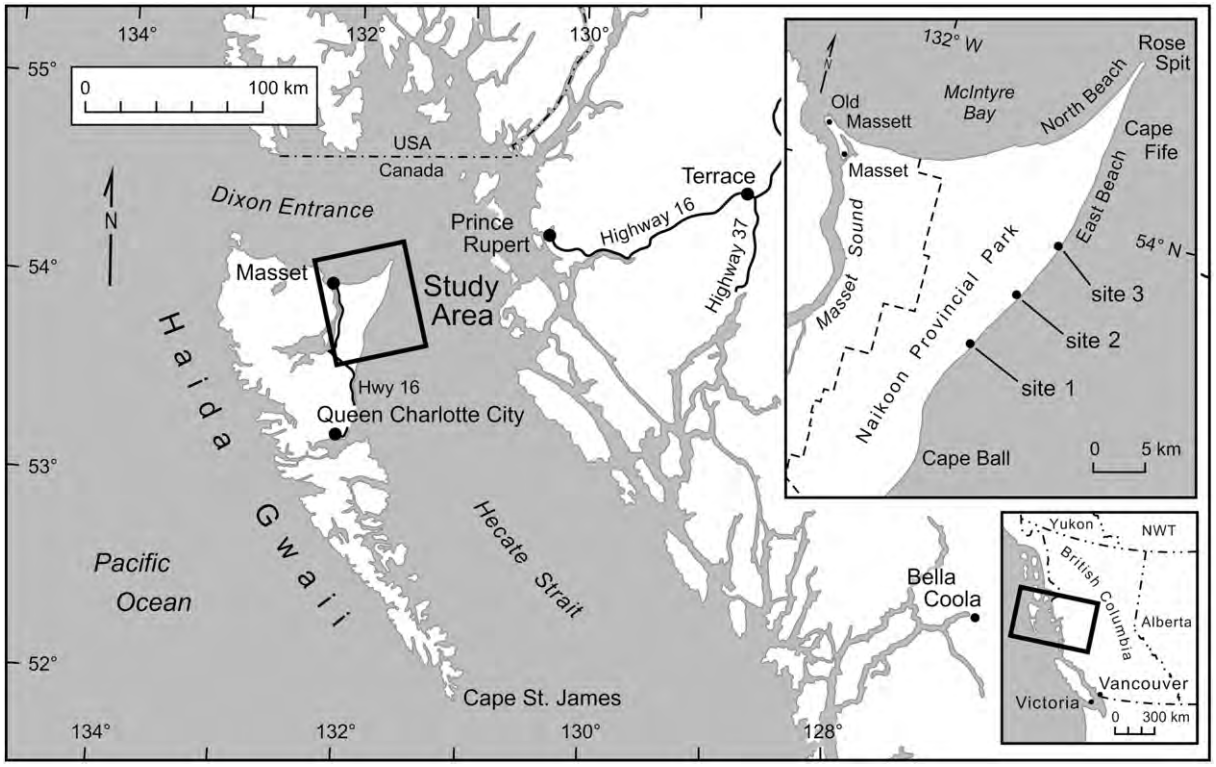


**Fig. 4.** Study region on northeastern Graham Island, Haida Gwaii (Queen Charlotte Islands), British Columbia. Three study sites are located on East Beach in Naikoon Provincial Park.

Of all three sites, site one had the most dense, continuous LWD coverage with the least amount of sand deposition (Fig. 5). The beach at site one hosted regularly-spaced, coarse-grained cusps on a mixed gravelly sand beach-face and a sandy shore-attached intertidal bar that, during strong winds at lower tides, provided an additional source of aeolian sand. Along the seaward margin of the LWD deposit was an elevated storm berm capped with aeolian sands that marked the upper limit of storm wave swash. The landward margin of site one was demarcated by a scarped and vegetated established foredune indicative of a historical erosive high water event and subsequent deposition of log debris in the backshore.

Site two (Fig. 6) had a similar gravelly sand beach-face with a discontinuous, gravelly shore-parallel intertidal bar just below the spring high tide line. The LWD deposit had little vegetation cover, greater aeolian deposition than site one, and the landward foredune scarp was less distinguishable. Most distinct were the large, transgressive bluff-top dunes that have migrated into the forest (cf. Hesp and Short, 1999). Although these dunes have a parabolic shape and align with the dominant southeasterly winter winds, they are not parabolic dunes proper as they do not have distinct vegetated arms or an identifiable deflation plain.

Site three (Fig. 7), the northernmost of the study sites, had the most sand deposition and vegetation colonization within the LWD deposit and, as such, hosted a well-developed incipient foredune. The established foredune backing site three had a well-developed scarp fill ramp and distinct blowouts aligned with the dominant southeasterly storm winds, with depositional lobes that have migrated into dense forest cover.

## 3. Methods

### 3.1. Overview of developed methodology

To quantify the sand storage capacity of LWD on a sandy beach, a novel method was developed that combined precise LiDAR digital elevation data with coincident, high-resolution digital orthophotos. The LiDAR data were separated into two distinct elevation datasets (sand and woody debris) by performing a ground cover classification using the digital orthophotos. In doing so, the geographic coordinates of the LiDAR data to this point were not modified or interpolated in any way. The resulting LiDAR datasets were then used to develop digital elevation models (DEMs) for each surface. Using these surfaces and a baseline datum (HHWMT), the existing and potential relative sand storage capacities ($C_E$ and $C_P$, respectively) within LWD was calculated for each study site. Details on the steps involved in these methods are described below.

### 3.2. LiDAR data collection and pre-processing

LiDAR data and coincident digital orthophotographs were collected in July and September 2006 using a discrete return Mark II LiDAR system mounted on a fixed wing aircraft from an altitude of approximately 1300 m aMSL. The ground distance between laser pulses (laser post-spacing) for both missions was approximately 1.75 m across track (i.e., perpendicular to the direction of aircraft motion) and 2.4 m along track, which yielded a ground coverage density of 0.6 to 2.0 points $m^{-2}$ with a vertical accuracy of approximately 0.20 m. LiDAR data were georeferenced to UTM map projection (Zone 9 N) and the 1983 North American Horizontal Datum (NAD83) then corrected to metres above modern sea level (m aMSL) using the Canada 2000 Geoid HT 2.0 model.

### 3.3. Ground cover classification from digital aerial orthophotography

Digital orthophotographs covering approximately 1 km by 1 km were taken at 20 cm spatial resolution as 8-bit, three band (red, green and blue or RGB) raster images. Imagery was imported into PCI Geomatica™ (PCI) for site delineation, analysis, and classification. The boundaries of each study site were defined by a seaward boundary (recent high tide debris line) that reflects the transition from hydrodynamic to aeolian sediment transport mechanisms (Hughes and Turner, 1999) and a landward boundary defined by the interface between a backshore scarp and log debris. A bitmap polygon for each

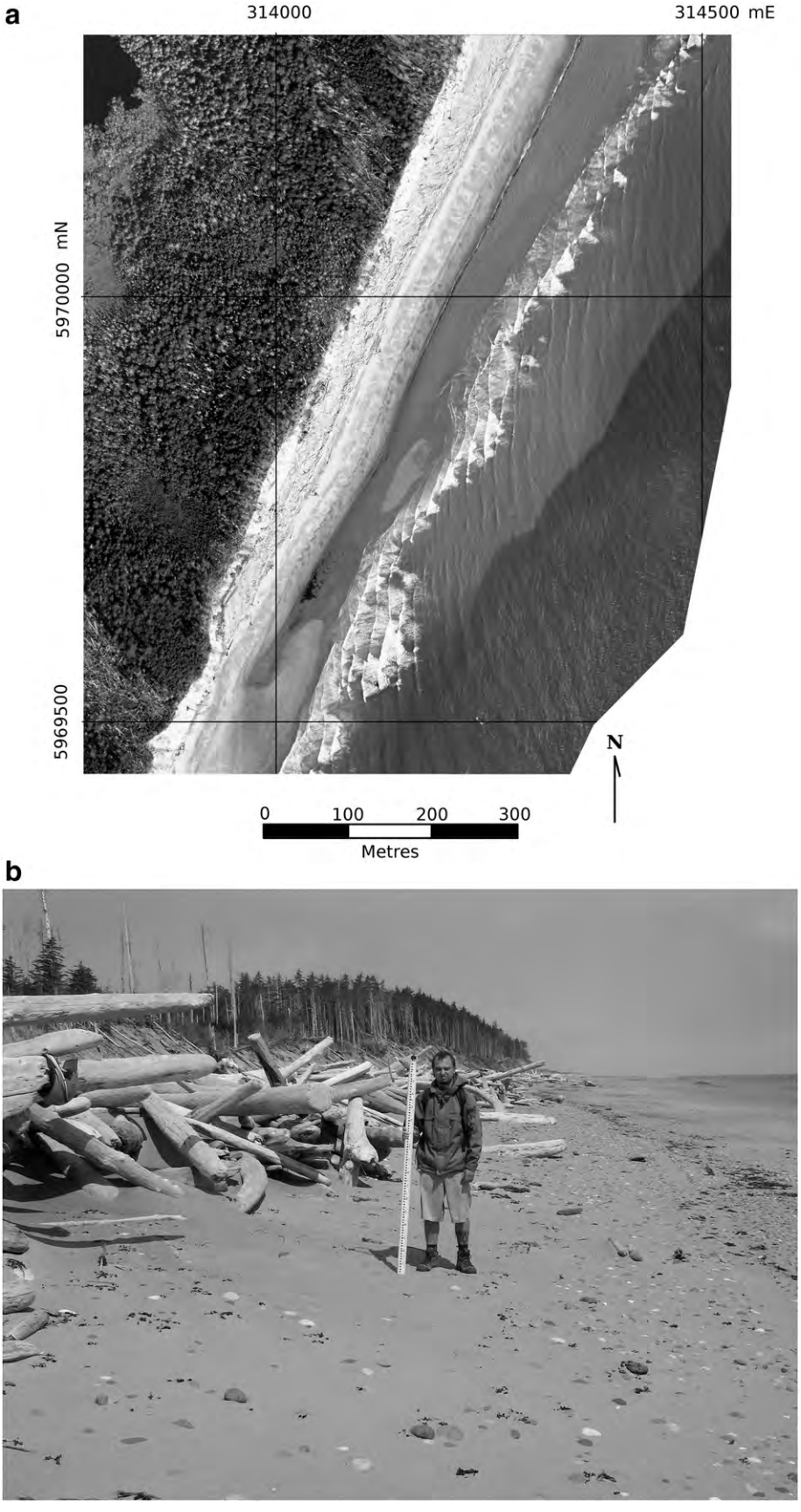


**Fig. 5.** (a) Aerial photograph of site one showing dense and continuous LWD coverage in the backshore and oblique shore-attached intertidal to subtidal bar. (b) Seaward edge of LWD near site 1 showing the distinct, steep (~1.5 m high) boundary formed by storm wave attack. Note also the deposition of aeolian sand from the upper beach within the LWD deposit. Photo credit: I.J. Walker.

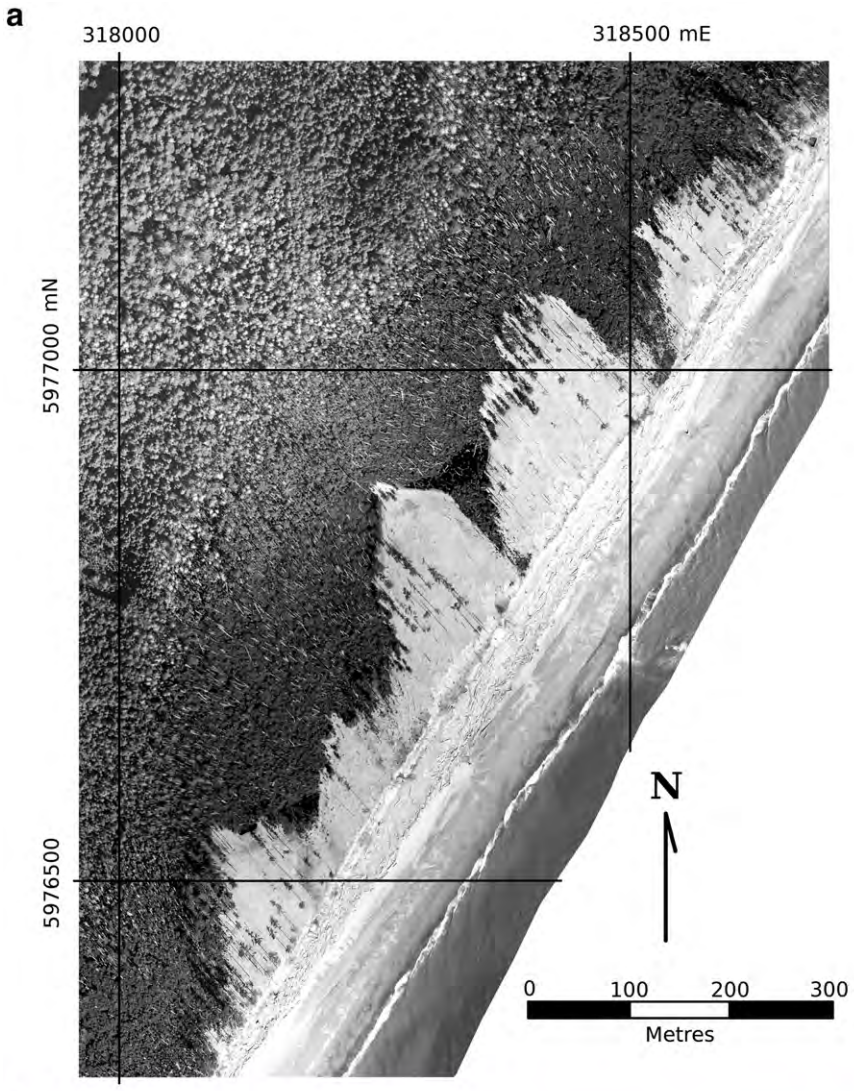
a
318000
318500 mE
5977000 mN
5976500
N
0
100
200
300
Metres


b

site was then created in PCI by adjoining landward and seaward boundaries with shore-normal transects.

A supervised classification was conducted in PCI to identify systematically two ground cover classes — sand surface and log debris. As both covers had similar spectral signatures, the supervised classification allowed for selection of training sites to classify each cover type using both image pixel statistics and visual truthing. Training sites for each cover type were delimited manually. Log training polygon bitmaps ranged in size from single logs to several tens of square metres depending on log density (Fig. 8). Sand training polygons were selected on the upper beach-face where log debris was not present and sediments were assumed to be relatively dry.

A minimum number of independent training pixels are required for supervised classification. For *N*-dimensional multispectral space, where an RGB air photo would have three dimensions (i.e., $N=3$), Swain and Davis (1978) recommended at least 10 N training pixels per ground cover class be used, with as many as 100 N if possible. This corresponds to 300 pixels per training class per image, which was met easily in this study.

Once training sites were outlined, the maximum-likelihood classification in PCI was used. Following this, a class editing procedure and a classification accuracy assessment were conducted. The class editing procedure involved the manual removal of clearly erroneous classification results by comparing the output with the unaltered orthophotographs. The majority of erroneously classified pixels were of the sand class near the low tide line, far from the LWD deposit. Following the procedure outlined in Jensen (2005), a random sampling accuracy assessment was conducted in PCI and produced overall classification accuracies of 93.33%, 92.67%, and 87.33% for sites one, two and three, respectively.

### 3.4. Separation of LiDAR data using ground cover classes

Before elevation surfaces for both sand and LWD classes could be created, ground cover pixel classes (in raster form) had to be assigned to elevation values from the LiDAR data (in vector form) with minimal loss of spatial data resolution or accuracy. The first step involved using PCI to export the classified raster image as an ASCII grid file containing classified grid values of 0 for null (outside of the study site), 1 for LWD, and 2 for sand. Second, a C# script was written to assign known UTM coordinates to each grid value in the ASCII. This produced a file containing point data with UTM coordinates and a ground cover classification value. At this stage, both the classified ground cover dataset and the LiDAR dataset were converted to similar point data file structures (i.e., positional coordinates and attribute values).

The third step involved assigning a cover class from the ground cover dataset to the irregularly spaced LiDAR data. To do so, another C# script was written to identify the corresponding cover class for each LiDAR data point by comparing the two point data files. Conceptually, as each LiDAR data point lay within a pixel area, the script identified the ground cover class of the corresponding pixel and assigned it to the LiDAR data point. The resulting dataset contained the original LiDAR data points (UTM coordinates and elevation) and a ground cover class (1 for LWD, 2 for sand). This process was repeated for each site.

### 3.5. Digital surface models and sand storage capacity calculations

The classified LiDAR datasets for each site, described above, were imported into three-dimensional graphing software (Golden Software's Surfer™, version 8.0). Data were gridded and interpolated to create digital elevation models for each study site. Separate surfaces were also created for sand and LWD classes to allow for sand storage capacity estimation by comparing volumes between interpolated surfaces. The kriging interpolation method was chosen as it is appropriate for irregularly spaced data produced by LiDAR surveys (Zhang et al., 2005). A 10-m radius search ellipse was chosen by trial-and-error, as it provided an optimal balance between the creation of unnecessary holes in the grid and over-representation of the data. A surface spatial resolution (i.e., output grid spacing) of 2 m was used, as it matched approximately the point density of the original LiDAR data and because this spacing is adequate to characterize many coastal geomorphic features (Woolard and Colby, 2002).

A baseline horizontal datum of the highest high water mean tide (HHWMT) level was chosen for volumetric calculations as it defines the highest average vertical extent of the swash zone. Above this datum, it is assumed that aeolian processes dominate sediment transport and deposition. Although this is an oversimplification, more complex modeling of a baseline surface (e.g., convex or sloping profile) for each site was beyond the scope of this study. HHWMT and mean sea level (MSL) elevations for Cape Ball (see Fig. 4) of 6.07 m and 3.82 m above nautical chart datum, respectively, were obtained from the Canadian Hydrographic Service. Thus, HHWMT is 2.25 maMSL and this elevation defines the basal horizontal surface above which relative sand storage capacities are calculated. This is presented conceptually in Fig. 9.

On a beach laden with LWD, the volume of material contained above this basal datum includes both woody debris and sand. As such, the actual volume of sand stored within LWD cannot be determined without knowing the volume of buried woody debris, which was not possible to measure. Instead, two relative storage "capacities" were quantified that represent the amount of LWD debris and sand stored above HHWMT. First, an existing relative storage capacity, $C_E$, was calculated as the volume of material above a horizontal plane defined by the HHWMT datum to the classified sand surface DEM, which includes the LWD-free beachface. Second, a potential relative storage capacity, $C_P$, was determined as the volume of material between the classified sand surface DEM and the LWD DEM. Both quantities were calculated by the graphing software. Because the $C_E$ values for each site include the beachface, they are inherently greater than $C_P$ values. Furthermore, as the LWD DEM is generally higher than the sand surface DEM, the $C_P$ is a proportional measure of the future volume of aeolian sand that could be trapped within the LWD (Fig. 9).

To compare values across the three study sites, relative storage volumes were normalized using shoreline width (Table 1) and the bulk density of sand (1600 kg $m^3$, Arens, 2004) to produce a storage mass term in kg $m^{-1}$ beach width. Values were also normalized by the surface area of each site to produce a relative storage depth in metres. For $D_E$, the $C_E$ value was divided by the area of the classified sand surface DEM, which includes the beachface to the HHWMT elevation. For $D_P$, the surface area of the classified LWD DEM was used to produce a potential storage depth within the LWD. As such, as the $D_P$ value reaches zero, the LWD becomes completely filled with sand. Resulting normalized storage mass and depth values are thus independent of the size of each site (Table 2).

Uncertainty values for storage capacity values were calculated using the +/−20 cm vertical accuracy for the LiDAR elevation data applied over the total DEM area of each study site to produce an uncertainty volume. These volumes were converted to a relative accuracy (percentage) by dividing the total volume of the unclassified DEM above HHWMT by the uncertainty volume. This produced relative accuracies of 10.5, 13.3, and 13.9% for sites one, two and three, respectively. Relative accuracy values were then multiplied by estimated storage capacity volumes to obtain absolute volumetric accuracies (see +/− values in Table 2). The LiDAR vertical accuracy was also used directly as the error range for area normalized storage depth values.

**Fig. 6.** (a) Aerial photograph of site two showing LWD coverage with an intermediate deposition of aeolian sands and distinct bluff-top dunes migrating landward into forest stand. (b) Ground photo showing discontinuous coverage of LWD and small dunes forming within the log matrix. Photo credit: I.J. Walker.

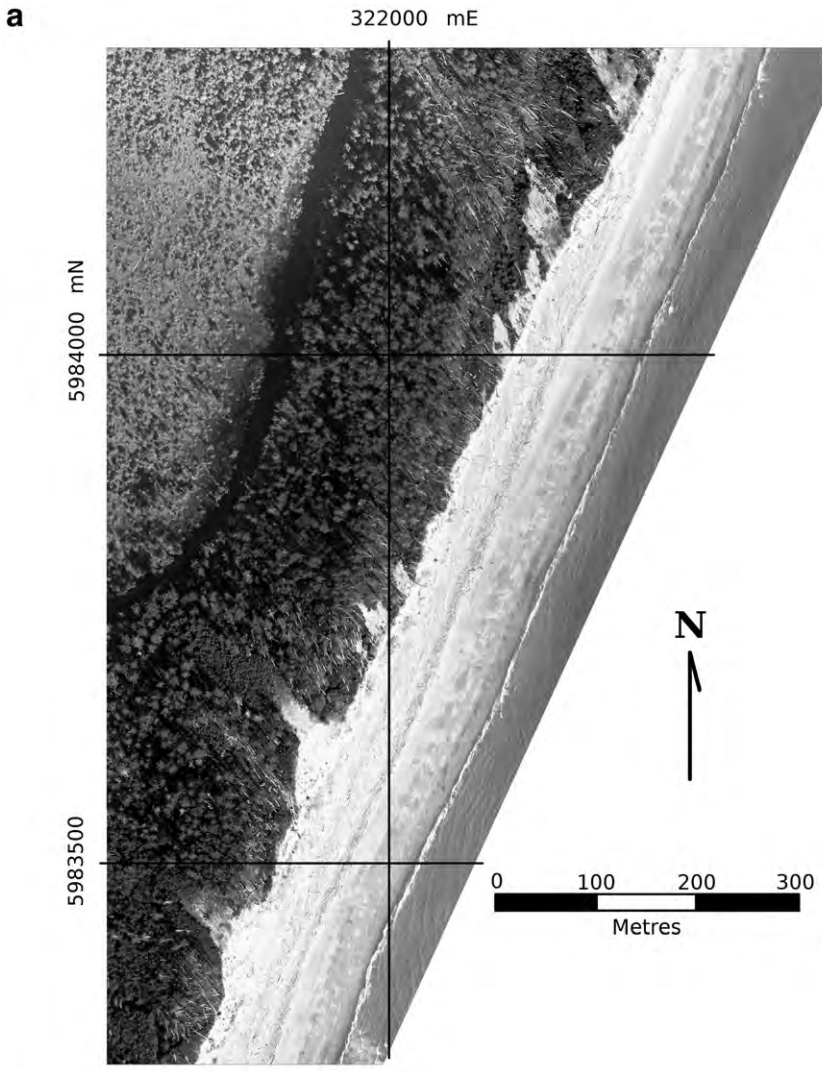
a
322000 mE
5984000 mN
5983500
N
0
100
200
300
Metres


b

**Table 1**
Study site location and general parameters.

| Site | 1 | 2 | 3 |
|---|---|---|---|
| UTM coordinates (NE corner, zone 9) | 313750 m E 5970300 m N | 317500 m E 5976300 m N | 321500 m E 5983300 m N |
| Latitude and longitude (NE corner) | 53.85°N 131.83°W | 53.90°N 131.78°W | 53.97°N 131.72°W |
| LWD-backed shoreline width (m) | 800 | 1010 | 1080 |
| Average cross shore depth of beach (m) | 88 | 85 | 110 |
| Average cross shore depth of LWD (m) | 32 | 26 | 43 |
| LWD density and continuity | Dense, continuous | Intermediate, discontinuous | Sparse, continuous |

## 4. Results

### 4.1. Existing and potential relative storage of sand and LWD

Existing and potential relative storage capacities ($C_E$ and $C_P$) and depths ($D_E$ and $D_P$) are presented in Table 2. Although site three had the largest surface area and thus the greatest existing relative storage capacity ($C_E = 94{,}160 +/- 13{,}088\ m^3$), site one had the largest existing relative storage depth ($D_E = 1.60 +/- 0.20$ m) normalized by area, and the same relative storage mass per unit beach width ($C_E - 1.39 \times 10^5\ kg\ m^{-1}$) as site three. Site one also had the highest potential storage capacity ($C_P = 8498 +/- 892\ m^3$), depth ($D_P = 0.28 +/- 0.20$ m) and mass per unit beach width ($C_E = 1.70 \times 10^5\ kg\ m^{-1}$), which is consistent with observations of limited sediment deposition within the deep LWD deposit at this site. Site two had the lowest existing and potential storage capacities ($C_E = 58{,}001 +/- 7724\ m^3$, $C_P = 6538 +/- 870\ m^3$), the smallest existing storage depth ($D_E = 1.14 +/- 0.20$ m), and the lowest existing and potential storage mass per unit beach width ($C_E = 9.19 \times 10^4\ kg\ m^{-1}$, $C_P = 1.04 \times 10^4\ kg\ m^{-1}$). This is consistent with the appreciable observed sediment deposition within the LWD and sediment bypassing that has maintained the large, transgressive bluff-top dunes backing this site. Sites two and three had comparably low potential storage depths and mass per unit beach width. The high existing storage capacity and least potential storage depth at site three is consistent with observations of significant sediment deposition in an incipient foredune developing within and around the LWD at this site.

### 4.2. Sand and LWD DEM surfaces and morphological interpretations

Shaded contour maps of the classified sand and LWD ground cover DEMs, storage depth, and a classified land cover surface for each site are shown in Fig. 10a, b, c. Sand surface maps show essentially the surface morphology of the $C_E$ while LWD surface maps shows the upper limit of woody debris protruding above sand (see also Fig. 9). The storage depth surface is the difference between LWD and sand surface elevations, which shows the spatial distribution of $D_P$. The classified land cover surface shows sand and LWD ground cover classes. Comparison of these maps allows for interpretation of the relationship between LWD and sand deposition within the backshore.

In general, site one has the highest potential sand storage capacity as seen in the storage depth map, highest $C_P$ and $D_P$ values, and high density of classified LWD roughness surface. In contrast, site three has the lowest potential sand storage capacity, using the same respective sources of information. Orthophotos of sites two and three show evidence for sediment bypassing the LWD (Figs. 6, 7) in large bluff-top dunes and blowouts.

A distinct shore-parallel ridge capped with appreciable amounts of aeolian sand exists on the seaward edge of all sites (Fig. 10a, b, c) and is most evident at site one (Fig. 5b). Comparison of sand, LWD, and storage depth surfaces with orthophotos and ground surveys suggest this is an incipient (albeit unvegetated) foredune (vs. swash-formed beach ridge) developing within the LWD matrix. Storage depths are generally high, reflecting a raised ridge or rampart of LWD, initially formed by piling of logs at the upper limit of storm wave swash. It is likely that high amounts of sand deposition occur within this feature due to abrupt flow stagnation and surface roughness effects that reduce the competence of sand transport locally. This incipient LWD foredune ridge becomes less prominent at sites two and three.

Drift logs are also deposited as far back as the scarp in the established foredune at all sites. This scarp, and the largely historical LWD (i.e., logging debris) deposited seaward of it, are clear evidence that higher water levels have occurred historically to completely rework and redeposit log debris at each site. Linear to curvilinear ridges between the foredune scarp and beach at each site also indicate LWD deposition and/or reworking has occurred during subsequent high water events.

## 5. Discussion

### 5.1. Methodological implications

This study provides a novel method to estimate existing and potential sand storage capacity within LWD deposits on beaches using remotely sensed data and shows that these features can trap significant amounts of aeolian sand in areas with high onshore sand supply. This method allows for development of separate, precise DEMs of different land cover classes using coincident LiDAR data and digital orthophotography. From these maps and a baseline datum, estimates of relative sand storage capacities are possible.

The existing storage capacity, $C_E$, is simply the combined volume of sediment and wood debris stored in a beach above HHWMT and, as such, it is only a relative measure of sand storage volume. Likewise, the potential storage capacity, $C_P$, is only a relative measure of the maximum volume of sand that could be stored within the LWD deposit as defined by the upper surface of logs protruding from the beach. Relative storage depth and mass values normalize these quantities by surface area and beach (shoreline) width to allow for inter-site comparison. Recognizing the difficulty in estimating log volumes within the sand–LWD matrix, these quantities are meant to provide order of magnitude estimates of sand storage that are useful for coastal sediment budget or mass balance calculations. Provided that suitable baseline data can be defined, this method is also useful for quantifying sand storage within established and incipient foredunes and blowouts in other areas laden with LWD.

### 5.2. Implications for beach–dune sediment budgets and geomorphology

As much of the woody debris on the west coast of North America is derived from logging, the impacts of LWD on beach–dune sediment budgets and geomorphology are largely historical. Prehistorically then, assuming a similarly energetic wind regime, high onshore sand supply, and absence of LWD, a much higher volume of sand could have been transported beyond the upper beach to feed more active and/or migrating foredune and parabolic dunes. Although some of the stabilized prehistoric foredunes backing the shoreline are larger (Wolfe et al., 2008), it is difficult to ascertain whether or not this related to an absence of backshore roughness (LWD) or varying wind regime, sand supply, or beach width conditions.

Currently, LWD deposits in the study region have been observed to completely fill with sand following their deposition within seasons to

**Fig. 7.** (a) Aerial photograph of site three showing appreciable aeolian sand deposition within the LWD deposit and distinct blowouts and bluff-top dunes that have migrated into dense forest cover. (b) Ground photo of LWD deposit nearly filled with aeolian sand with early sparse colonization by native dune grass (*Leymus mollis*) and larger hummocks of invasive beach grass (*Ammophila* spp.). Person holding survey rod for scale. Photo credit: I.J. Walker.

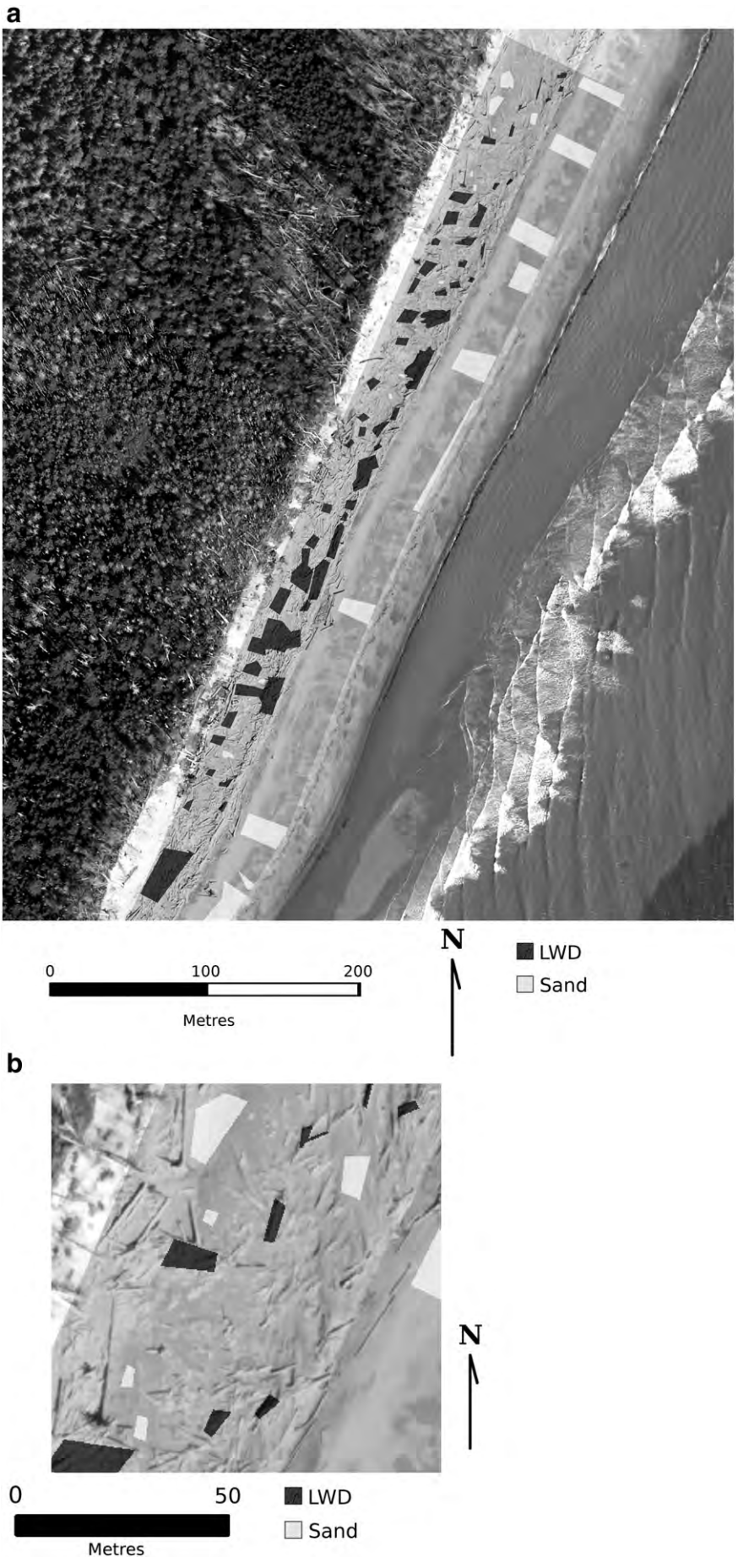
a
0
100
200
Metres
N
LWD
Sand
b
0
50
Metres
N
LWD
Sand

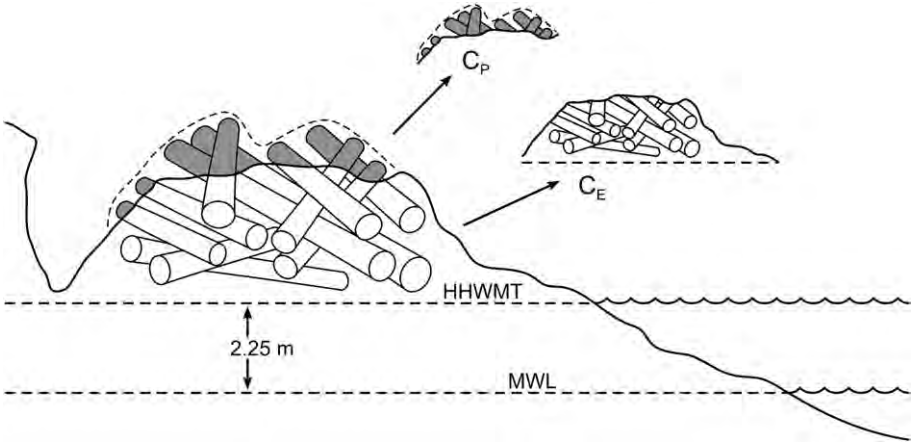


**Fig. 9.** Stylized diagram of a backshore LWD deposit partially filled with aeolian sands showing existing ($C_E$) and potential ($C_P$) storage capacities. The lower boundary for the $C_E$ is the highest high water mean tide (HHWMT) elevation (2.25 m aMSL), which is assumed to be the upper limit of wave swash processes. The existing sand surface serves as the upper boundary for the $C_E$ and the lower boundary for the $C_P$. The upper boundary for potential storage capacity is delimited by an interpolated surface connecting all protruding log debris. The potential storage depth, $D_P$, is calculated using the elevation difference between $C_P$ and $C_E$ surfaces.

**Table 2**
Existing and potential relative storage capacity ($C_E$ and $C_P$) and relative storage depth ($D_E$ and $D_P$) quantities including corresponding surface areas and uncertainty terms. Values are expressed as volumes ($m^3$), depths (m) normalized by surface area, and a storage mass (kg $m^{-1}$) normalized using a bulk density of 1600 kg $m^{-3}$ and shoreline widths provided in Table 1.

| Quantity | Site | | |
|---|---|---|---|
| | 1 | 2 | 3 |
| $C_E$ surface area ($m^2$) | 43,677 | 51,021 | 66,956 |
| $C_E$ ($m^3$) | $69678 \pm 7316$ | $58001 \pm 7724$ | $94160 \pm 13088$ |
| $C_E$ (kg $m^{-1}$) | $\sim 1.39 \times 10^5$ | $\sim 9.19 \times 10^4$ | $\sim 1.39 \times 10^5$ |
| $D_E$ (m) | $1.60 \pm 0.20$ | $1.14 \pm 0.20$ | $1.41 \pm 0.20$ |
| $C_P$ surface area ($m^2$) | 29,759 | 29,932 | 34,650 |
| $C_P$ ($m^3$) | $8498 \pm 892$ | $6538 \pm 870$ | $7284 \pm 1012$ |
| $C_P$ (kg $m^{-1}$) | $\sim 1.70 \times 10^4$ | $\sim 1.04 \times 10^4$ | $\sim 1.08 \times 10^4$ |
| $D_P$ (m) | $0.28 \pm 0.20$ | $0.22 \pm 0.20$ | $0.21 \pm 0.20$ |

years (Walker and Barrie, 2006). As such, these features play a significant and changing role in the modern coastal sediment budget. This occurs because LWD increases the surface roughness and, in higher densities, induces flow stagnation effects that promote deposition of aeolian sands in the backshore. These deposits trap significant amounts of sand — as much as $9.19 \times 10^4$ to $1.39 \times 10^5$ kg $m^{-1}$ beach width or ~1.14 to 1.60 m storage depth above HHWMT — and offer a appreciable additional (potential) storage capacity as high as $1.70 \times 10^4$ kg $m^{-1}$ beach width or ~0.28 m depth.

Although LWD deposits effectively reduce sand supply to more distal established dunes at higher elevations in the backshore, a significant amount of sand (up to 110 kg $m^{-2}$ during the fall–winter storm season) can still be transported hundreds of metres landward of the LWD during storm winds to produce metres of vertical accretion on established dunes in the study area (Pearce, 2005; Anderson and Walker, 2006). This is evidenced by large, transgressive bluff-top dunes and blowouts seen landward of sites two and three.

A large proportion of aeolian sand within the study area is deposited within the log matrix to form sizable, often unvegetated, incipient foredunes at relatively low elevations on the backshore. In some locations, vegetation colonizes sheltered areas of the LWD-laden foredune rapidly, while in other more exposed locations sizable incipient dunes form and are maintained interannually with no vegetation cover. This type of 'roughness-initiated' dune form is unlike typical vegetation-dependent incipient foredunes (cf. Hesp, 1989) and has not been documented in the literature.

Aeolian sand stored within LWD on the backshore has greater exposure to erosion by wave attack than if it were delivered to landward established dunes. However, as these LWD deposits and incipient dunes must be reworked first during high water events, they provide an important buffer that may reduce erosion of established foredunes along this coast.

On a prograding coastline with a positive sediment budget (i.e., net onshore sand supply), it would follow that LWD could enhance protection against erosion caused by increasing storminess and sea-level rise. Despite high onshore aeolian sand transport and extensive LWD in the study region, however, the historical aerial photograph record shows that this coastline has retreated at ~1 to 3 m $a^{-1}$ (Barrie and Conway, 2002). Relict scarps in established foredunes behind the LWD deposits and rapidly retreating bluffs elsewhere along this coast suggest that high water events and complete reworking of LWD deposits occur, perhaps on an interdecadal scale. Due to the comparatively rapid redeposition of LWD and aeolian sand, however, these features have been maintained historically, although their size, location, and storage capacity have changed.

Since the 1970s, extreme water level events have increased at a rate of ~3.4 mm $a^{-1}$ in response to ENSO and PDO climatic variability events, which is more than twice the rate of regional sea-level rise (1.4 mm $a^{-1}$) (Abeysirigunawardena and Walker, 2008). In 2007, all study sites were eroded to at least half of their cross-shore depth and site three was removed almost completely. This suggests that the future ability of these LWD deposits to re-establish, trap sediment, and buffer this coastline may be challenged by future climatic variability and change impacts.

## 6. Conclusions

This study provides a novel method to quantify existing and potential sand storage capacity within large woody debris deposits on beaches using remotely sensed LiDAR data and digital orthophotos. Results show that LWD can trap significant amounts of aeolian sand in areas with high onshore sand supply. As far as the authors are aware, this is the first study to quantify sand storage capacity within large woody debris on beaches and explore geomorphic implications. Key conclusions are as follows:

1) A new method for developing precise DEMs of different land cover classes (sand and LWD) from a single dataset of coincident LiDAR

**Fig. 8.** (a) Northern portion of site 3 showing training site polygons for classification of LWD (dark grey) and sand (white) land cover classes. The larger grey polygon delineates the larger study site. (b) Magnification of training sites from (a) showing the variation in training site polygons and discrete LWD features and sand patches in the image.

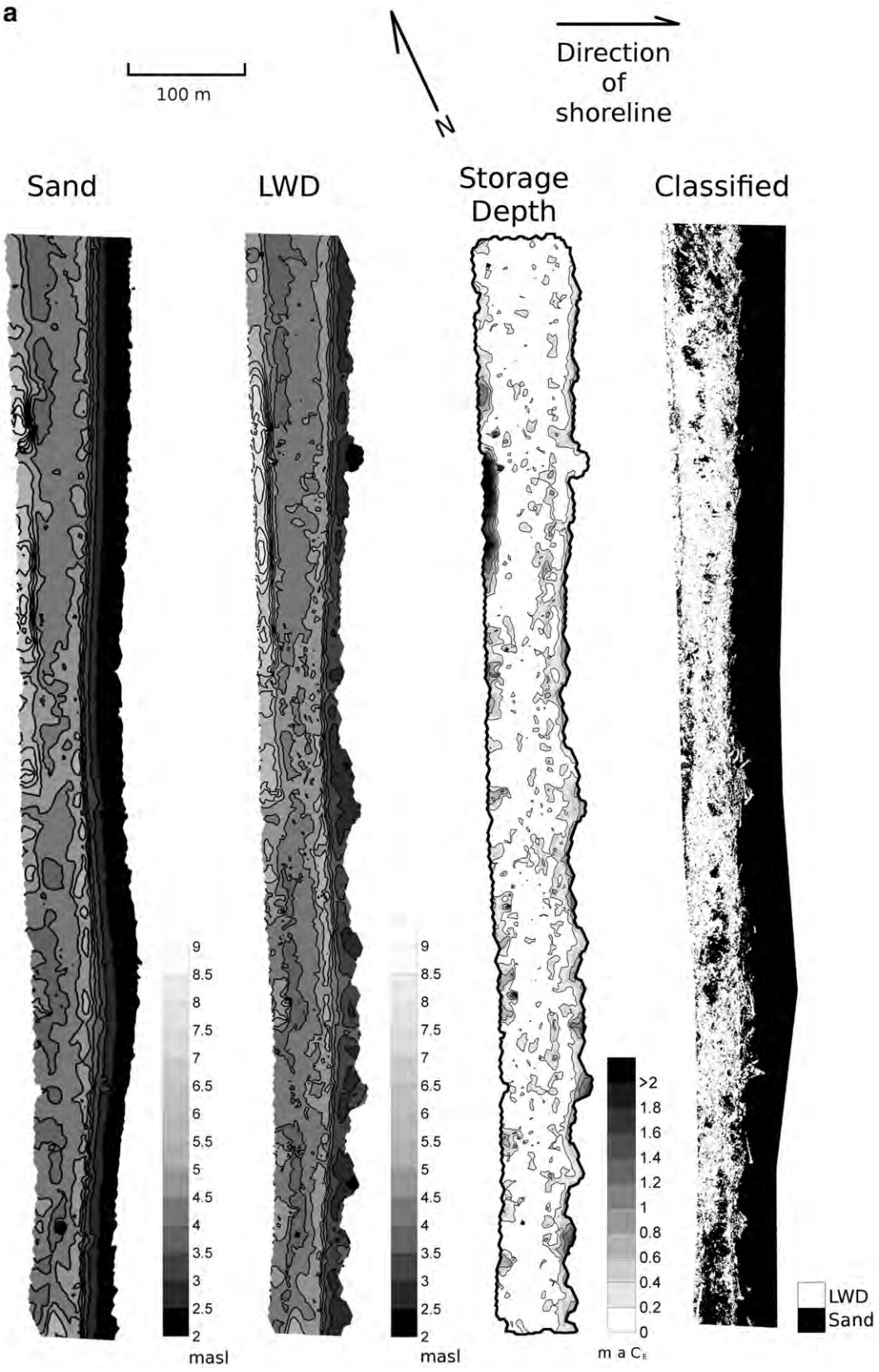


**Fig. 10.** Maps of sand and LWD elevation surfaces, storage depths, and classified land cover classes for (a) site one, (b) site two, and (c) site three. Sand surface maps represent the surface morphology of the $C_E$. LWD surface maps represent the upper elevations of woody debris protruding above the sand (see also Fig. 9). The storage depth surface is calculated as the difference between LWD and sand surface elevations, displaying the spatial distribution of $D_P$. The classified land cover surface shows sand and LWD ground cover classes.

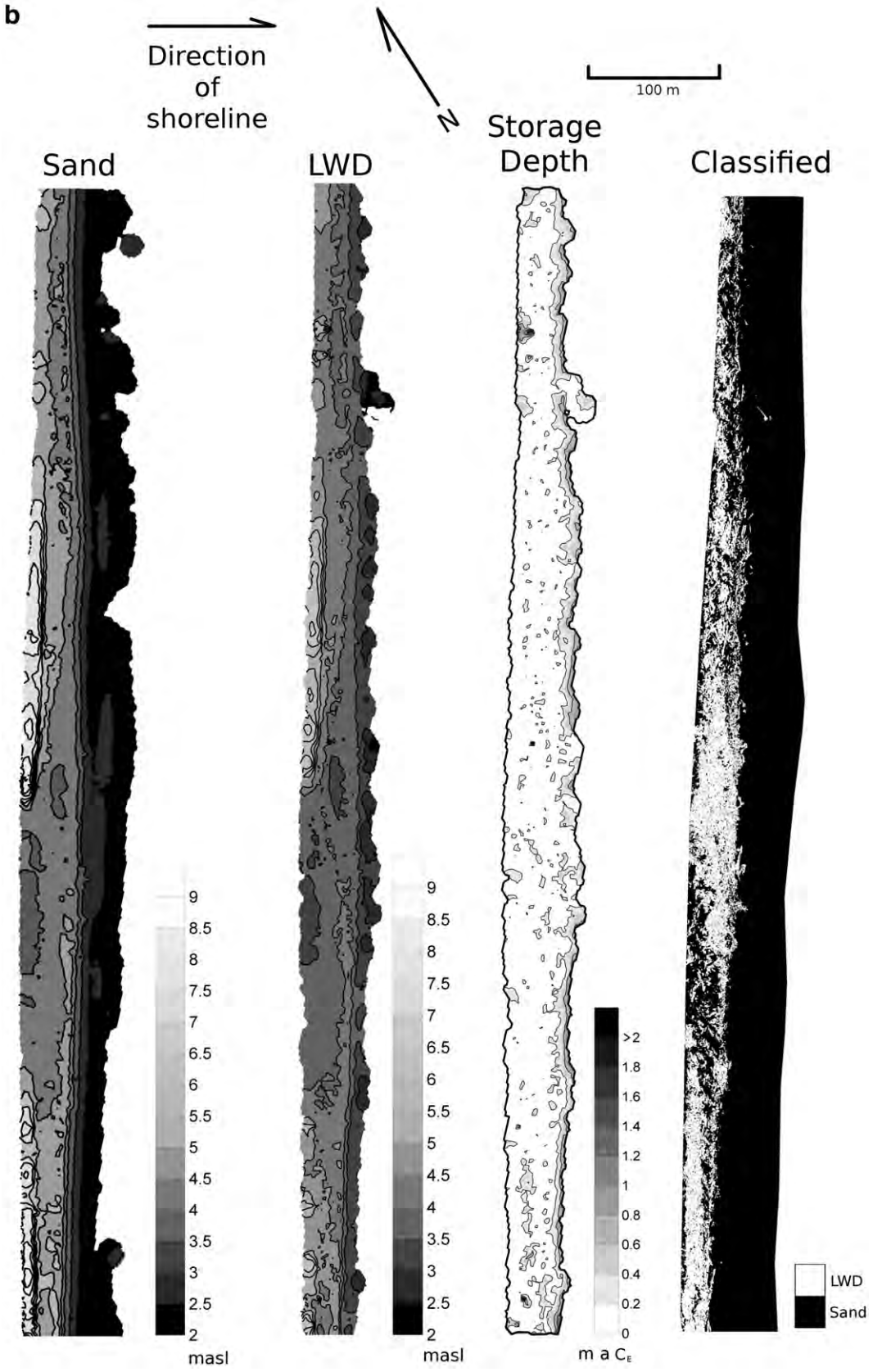


**Fig. 10** (*continued*).

and digital orthophotography is developed that provides precise, order-of-magnitude estimates of existing and potential (maximum) sand storage capacities within LWD deposits on beaches.

2) Large woody debris increases aerodynamic surface roughness and, in higher densities, causes flow stagnation effects that promote deposition of aeolian sands in the backshore. Significant amounts of

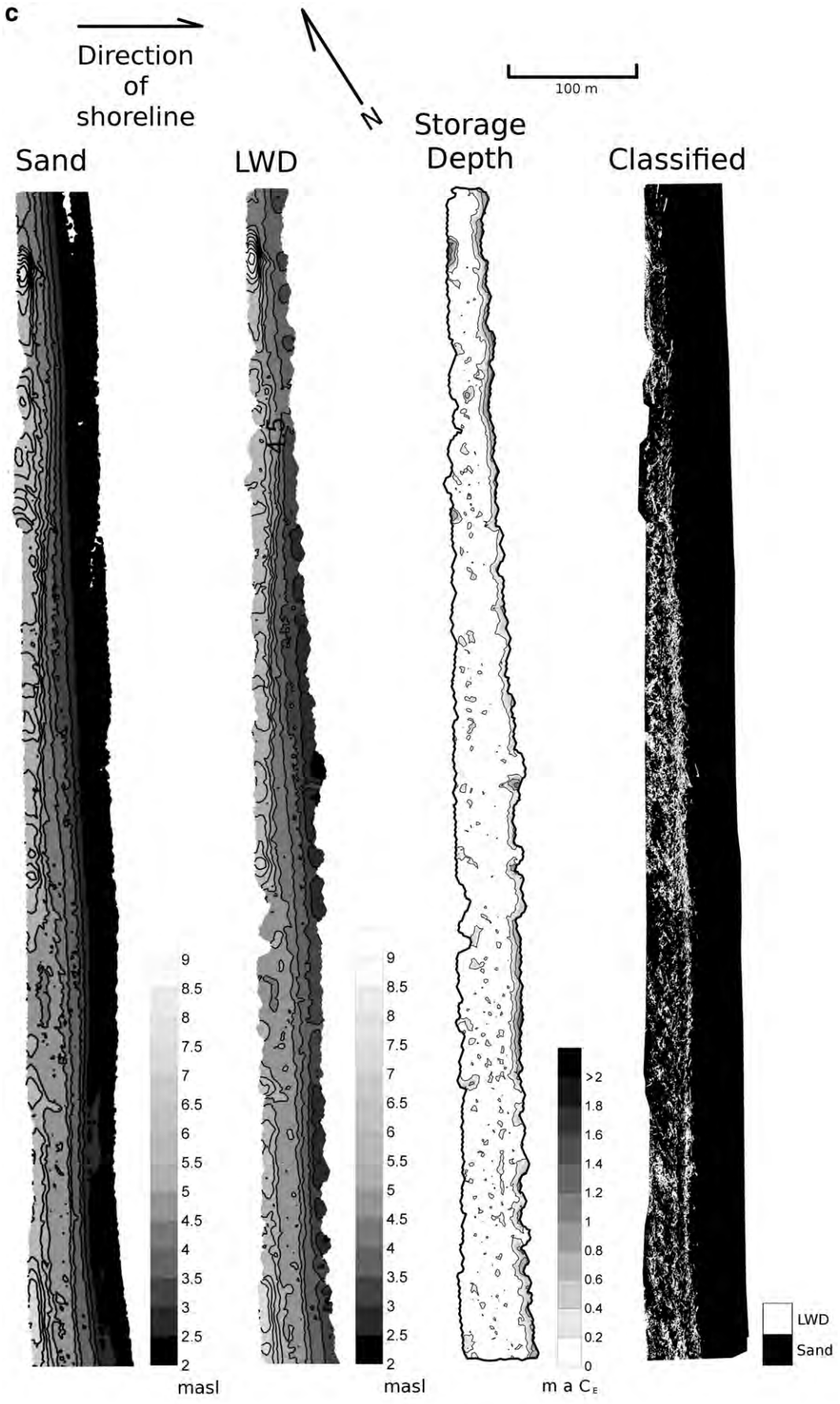


**Fig. 10** (*continued*).

sand are stored within LWD on beaches in the study region. Existing storage quantities (above HHWMT) range from $9.19\times10^4$ to $1.39\times10^5$ kg m$^{-1}$ beach width or ~1.14 to 1.6 m storage depth. The same LWD deposits have a potential storage capacity ranging from 1.04 to $1.70\times10^4$ kg m$^{-1}$ beach width or ~0.21 to 0.28 m depth.

3) As most of the LWD on beaches in the study area is a historical artifact of the logging industry, it is expected that much higher volumes of sand would have been transported prehistorically beyond the beach to feed more active and/or migrating dunes. This assumes similar wind regime and sand supply conditions as today and is potentially evidenced by larger, relict foredunes and parabolic dunes in the study area.

4) In the modern setting, sizable, unvegetated incipient foredunes form within LWD at relatively low elevations on the backshore. Although this material has a greater exposure to erosion by wave attack than established dunes landward of the LWD, it must be reworked first during high water events and, as such, provides an important buffer that may reduce erosion of established foredunes. Observations of relict scarps in established foredunes behind the LWD deposits, and rapidly retreating bluffs elsewhere in the study region, however, suggest that erosive high water events that completely rework LWD deposits may occur on an interdecadal scale. This, coupled with current trends in shoreline retreat, extreme annual water levels, and sea-level rise suggests that the ability of accreting LWD deposits to buffer this shoreline against future climatic variability and change impacts is limited.

## Acknowledgements

All C# scripts written for this research were developed with the advice and skill of Brendan Eamer. Dr. Eddie Loos was of great assistance with refining the land-cover classification and contributed valuable reviews to early drafts of this work. LiDAR and orthophoto data collection were funded by Natural Resource Canada's Climate Change Impacts and Adaptations Program (Project A580) and analyses were supported with funding from the Canada Foundation for Innovation, a Natural Sciences and Engineering Research Council (NSERC) Discovery Grant to IJW, and a NSERC-USRA grant to JBRE. LiDAR data and orthophotos were flown by Terra Remote Sensing, Sidney, British Columbia. Imagery mosaics and LiDAR data processing were provided by Olaf Niemann and the Hyperspectral LiDAR Research Group, Department of Geography, University of Victoria. Site access and research permits were granted by BC Parks and the Council of the Haida Nation. Comments from two anonymous reviewers were also very helpful in revising this manuscript.

## References

Abeysirigunawardena, D.S., Walker, I.J., 2008. Sea level responses to climate variability and change in northern British Columbia. Atmosphere-Ocean 46, 277–296.

Anderson, J.L., Walker, I.J., 2006. Airflow and sand transport variations within a backshore-parabolic dune plain complex: NE Graham Island, British Columbia, Canada. Geomorphology 77, 17–34.

Bagnold, R.A., 1941. The Physics of Blown Sand and Desert Dunes. Chapman & Hall, London.

Barrie, J.V., Conway, K.W., 2002. Rapid sea-level change and coastal evolution on the Pacific Margin of Canada. Sedimentary Geology 150, 171–183.

Brock, J.C., Wright, C.W., Sallenger, A.H., Krabill, W.B., Swift, R.N., 2002. Basis and methods of NASA Airborne topographic mapper LiDAR surveys for coastal studies. Journal of Coastal Research 18, 1–13.

Debruyn, W., Deronde, B., Fransaer, D., Henriet, J., Houthuys, R., Lancker, V.V., 2006. Use of airborne hyperspectral data and laserscan data to study beach morphodynamics along the Belgian Coast. Journal of Coastal Research 22, 1108–1117.

Hesp, P.A., 1989. A review of biological and geomorphological processes involved in the initiation and development of incipient foredunes. In: Gimmingham, C.H., Ritchie, W., Willetts, B.B., Willies, A.J. (Eds.), Coastal Sand Dunes. : Proceedings of the Royal Society of Edinburgh, vol. 96B. Edinburgh, pp. 181–202.

Hesp, P.A., Short, A.D., 1999. Barrier morphodynamics. In: Short, A.D. (Ed.), Handbook of Beach and Shoreface Morphodynamics. Wiley, London, pp. 253–288.

Hughes, M., Turner, I., 1999. The beach face. In: Short, A.D. (Ed.), Handbook of Beach and Shoreface Morphodynamics. Wiley, London, pp. 253–288.

Jensen, J.R., 2005. Introductory Digital Image Processing3rd edition. Pearson Prentice Hall, Upper Saddle River, NJ. 526p.

Kail, J., 2003. Influence of large woody debris on the morphology of six central European streams; interactions between wood and channel forms and processes. Geomorphology 51, 207–223.

Keller, E.A., Swanson, F.J., 1979. Effects of large organic material on channel form and fluvial processes. Earth Surface Processes 4, 361–380.

Lee, D.S., Shan, J., 2003. Combining LiDAR elevation data and IKONOS multispectral imagery for coastal classification mapping. Marine Geodesy 28, 117–127.

Maser, C., Sedell, J., 1994. From the forest to the sea: the ecology of wood in streams, rivers, estuaries, and oceans. St Lucie Press, Delray Beach, FL.

Nakamura, F., Swanson, F.J., 1993. Effects of coarse woody debris on morphology and sediment storage of a mountain stream system in western Oregon. Earth Surface Processes and Landforms 18, 43–61.

Pearce, K., 2005. Aeolian geomorphology of Northeast Graham Island, Haida Gwaii, British Columbia. MSc Thesis, University of Victoria, Canada.

Sallenger Jr., A.H., Krabill, W.B., Swift, R.N., Brock, J., List, J., Hansen, M., Holman, R.A., Manizade, S., Sontag, J., Meredith, A., Morgan, K., Yunkel, J.K., Frederick, E.B., Stockdon, H., 2003. Evaluation of airborne topographic LiDAR for quantifying beach changes. Journal of Coastal Research 19, 125–133.

Saye, S.E., van der Wal, D., Pye, K., Blott, S.J., 2002. Beach-dune morphological relationships and erosion/accretion: an investigation at five sites in England and Wales using LiDAR data. Geomorphology 72, 128–155.

Shrestha, R.L., Carter, W.E., Sartori, M., Luzum, B.J., Slatton, K.C., 2005. Airborne laser swath mapping: quantifying changes in sandy beaches over time scales of weeks to years. Photogrammetry and Remote Sensing 59, 222–232.

Swain, P.H., Davis, S.M., 1978. Remote Sensing: The Quantitative Approach. McGraw-Hill, New York, NY, USA.

Tsoar, H., 2000. The geomorphological background and paleogeography of the sand dunes that have formed the kurkar ridges in the coastal plain of Israel. Israel Journal of Earth Sciences 49, 189–196.

Walker, I.J., Barrie, J.V., 2006. Geomorphology and sea-level rise on one of Canada's most 'sensitive' coasts: Northeast Graham Island, British Columbia. Journal of Coastal Research SI 39, 220–226.

Wallerstein, N.P., Thorne, C.R., 2004. Influence of large woody debris on morphological evolution of incised, sand-bed channels. Geomorphology 57, 53–73.

Wolfe, S.A., Lemmen, D.S., 1999. Monitoring dune activity in the Great Sand Hills region, Saskatchewan. GSC Bulletin 534, 199–210.

Wolfe, S.A., Walker, I.J., Huntley, D.J., 2008. Holocene coastal reconstruction, Naikoon peninsula, Queen Charlotte Islands, British Columbia. Geological Survey of Canada, Current Research 2008–12, 16p.

Woolard, J.W., Colby, J.D., 2002. Spatial characterization, resolution, and volumetric change of coastal dunes using airborne LiDAR: Cape Hatteras, North Carolina. Geomorphology 48, 269–287.

Zhang, K., Whitman, D., Leatherman, S., Robertson, W., 2005. Quantification of beach changes caused by Hurricane Floyd along Florida's Atlantic coast using airborne laser surveys. Journal of Coastal Research 21, 123–134.